Journal of Molecular Catalysis A: Chemical 334 (2011) 65–76

Contents lists available at ScienceDirect

Journal of Molecular Catalysis A: Chemical

journal homepage: www.elsevier.com/locate/molcata

A kinetic model based on non-linear regression analysis is proposed for the degradation of phenol under UV/solar light using nitrogen doped TiO_2

L. Gomathi Devi*, K. Eraiah Rajashekhar

Department of Post Graduate Studies in Chemistry, Central College City Campus, Dr. Ambedkar Street, Bangalore University, Bangalore 560001, Karnataka, India

ARTICLE INFO

Article history:
Received 20 July 2010
Received in revised form 28 October 2010
Accepted 30 October 2010
Available online 5 November 2010

Keywords:
Nitrogen doped TiO_2
Ammonium persulfate
Kinetic/mathematical modeling
Phenol degradation

ABSTRACT

Nitrogen was doped into the TiO_2 matrix in the concentration range of 0.05–0.20 at.% and the photocatalytic activities were tested for the degradation of phenol (Ph) under UV/solar light using hydrogen peroxide (HP) and ammonium persulfate (APS) as electron acceptors. The prepared photocatalysts characterized by various analytical techniques confirm the incorporation of nitrogen in the TiO_2 lattice. The 0.15 at.% dopant concentration shows higher photocatalytic activity compared with sol–gel TiO_2 (SG) and Degauss P25 TiO_2 (P25) for the degradation process. Photoluminescence technique was used for studying the extent of hydroxyl radicals produced on TiO_2 and $TiO_{2-x}N_x$ (NT) surface in the presence of oxidants under UV/solar light irradiation. The kinetic rate equation obtained for the best system $TiO_{2-x}N_x$ ($x = 0.15$ at.%)/APS/under solar irradiation is found to be: $r_{ap,solar} = 0.0041[NT]^{0.54}[APS]^{0.71}[Ph]^{-0.70}$. A kinetic/mathematical model was developed based on the nonlinear regression analysis for the various processes and the validity of the model was tested by comparing the experimental values with the theoretically calculated data as a function of variable parameters like catalyst dosage, concentration of electron acceptors and initial concentration of Ph.

1. Introduction

TiO_2 mediated photocatalysis is promising technique and extensively used for the degradation of organic pollutants [1–6]. However the large band gap of TiO_2 (~3.26 eV) requires UV light to activate, also high degree of recombination between photogenerated charge carriers limits its overall photocatalytic efficiency. To minimize these problems, preparation of visible light active photocatalysts is an important viable approach in the field of photocatalysis. Doping with various transition metal ions is one of the effective approaches for synthesizing visible light active photocatalyst [7–12]. However better visible light response could be achieved by using non metal ion as a dopant [13–15]. In this regard various methods have been reported in literature for the incorporation of nitrogen in to the TiO_2 lattice [16–18]. The mechanism of response observed in the visible region is still under debate. Asahi et al. [17] reported that, the narrowing of the band gap by mixing of 2p states of nitrogen and oxygen mainly contributes for the response in the visible light. Irie et al. [13] reported that nitrogen doping formed a unique band above the valence band and the UV light would cause excitation from both bands while visible light could only excite the higher lying band. They reported that this effect would not be seen if the N 2p band over lapped with the valence band of the TiO_2 forming a single higher lying band. Irie et al. suggest the existence of localized states in the band gap for both substitution and interstitial nitrogen. The present research is focusing on the doping of nitrogen into the TiO_2 lattice. Its photocatalytic activity was investigated for the degradation of phenol (Ph) under UV/solar light using two symmetrical peroxides like hydrogen peroxide (HP) and ammonium per sulfate (APS) as electron acceptors. The results obtained were compared with the other catalysts like TiO_2 prepared by sol–gel method (SG) and commercially available Degauss P25 TiO_2 (P25). APS is proved to be a better electron acceptor compared to HP. The degradation process in the presence of catalyst and electron acceptors APS/HP under UV/solar illumination were analyzed and a kinetic/mathematical model was developed based on the nonlinear regression analysis and suitable rate expressions were proposed. Although these types of models were proposed for TiO_2 mediated photocatalytic process by few research groups [19–23] and Fenton's process by our research group [24], a detailed study is not attempted especially for the photocatalytic activity of nitrogen doped TiO_2 ($TiO_{2-x}N_x$) under UV/solar light irradiation in the presence of electron acceptor HP/APS. The validity of the model was

* Corresponding author. Tel.: +91 080 22961336.
E-mail address: gomatidevi_naik@yahoo.co.in (L.G. Devi).

1381-1169/$ – see front matter © 2010 Elsevier B.V. All rights reserved.
doi:10.1016/j.molcata.2010.10.025

Table 1
Powder X-ray diffraction, BET surface area and UV–visible diffusion reflectance spectral data of undoped TiO_2 (SG) and N doped TiO_2 catalysts at different concentrations of nitrogen.

Photo catalysts	D (nm)	(Å)	(Å)^3	λ_{max} (nm)	E_g (eV)	S_{BET}	
						S_{area} (m^2/g)	S_{sp} (cm^3/g)
SG	15.7932	$a=b=3.7828$ $c=9.5023$	135.97	380	3.27	18	0.36
NT1	40.3732	$a=b=3.7276$ $c=9.3953$	130.55	396	3.14	25	0.38
NT2	20.1266	$a=b=3.7184$ $c=9.3626$	129.45	416	2.99	32	0.59
NT3	15.7481	$a=b=3.7381$ $c=9.3581$	130.76	435	2.86	41	0.74
NT4	15.7456	$a=b=3.7368$ $c=9.3491$	130.55	424	2.93	36	0.68

D: crystallite size in nm, Å: lattice parameters, (Å)^3: unit cell volume, λ_{max}: absorption maxima in nm, E_g: band gap energies in eV, S_{BET}: BET characterization obtained by N_2 adsorption, S_{area}: surface area obtained by N_2 adsorption in m^2/g, S_{sp}: surface porosity in cm^3/g.

tested by comparing the experimentally observed and theoretically calculated data.

2. Experimental method

2.1. Materials

Titanium (IV) chloride ($TiCl_4 \geq 99.9\%$) was obtained from Merck Chemicals Limited, urea ($(NH_2)_2CO$) from Sisco-chemical Industries, Bombay. Phenol (C_6H_6O), APS and HP (50%, w/v) were supplied from SD Fine Chemicals, Bombay. Double distilled water is used for all the experiments.

2.2. Catalyst preparation

Anatase TiO_2 was prepared by sol–gel method through the hydrolysis of $TiCl_4$ as reported earlier [25]. A stoichiometric amount of urea solution was added to the calculated amount of TiO_2 powder to get the dopant concentration in the range of 0.05, 0.1, 0.15 and 0.2 at.%, which are abbreviated as NT1, NT2, NT3 and NT4 respectively. The mixture is ground in a mortar and oven dried at 120 °C for 1 h. The process of grinding was repeated for 4 times and the powder is finally calcined at 550 °C for 5 h. Doped TiO_2 powder shows pale yellow color. The nitrification of TiO_2 starts by the thermal dissociation of urea as represented by the following equation:

$$TiO_2 + \frac{x}{2}H_2N\text{–}CO\text{–}NH_2 \xrightarrow{\text{Grinding},\Delta} TiO_{2-x}N_x + xH_2O\uparrow + \frac{x}{2}CO\uparrow \quad (1)$$

In the processes of grinding, the crystal lattice of the TiO_2 undergoes deformation producing stress and strains, which creates a lattice distortion along with the creation of several defects inside the TiO_2 lattice. These defects produce high lattice distortion energy and they also increase the surface energy, thereby decreasing the activation energy for the diffusion of elements. This allows atomic or ionic diffusion at room temperature. When the activity of powder system is high enough, during the grinding process collision of grains in the powder may induce the chemical reaction. Higher the enthalpy of the reaction, more easily the reaction proceeds. The free energy of the system is lowered by converting mechanical energy of grinding into distortion energy and the defects in the powder lead to nitriding reaction to generate $TiO_{2-x}N_x$ [26].

Table 2
Nitrogen percentage obtained according to XPS analysis of undoped TiO_2 and nitrogen doped TiO_2.

Photocatalysts	XPS composition (at.%) Nitrogen (N)
SG	0.00
NT1	4.91
NT2	9.95
NT3	14.97
NT4	19.96

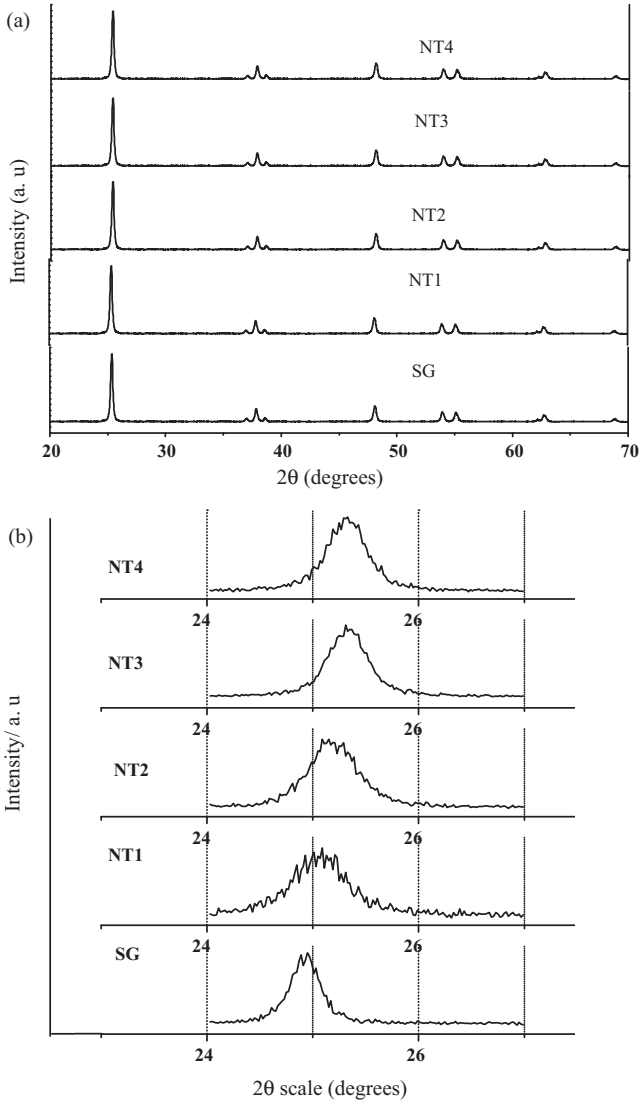

Fig. 1. (a) PXRD pattern of undoped TiO_2 (SG) and $TiO_{2-x}N_x$ photocatalysts for different concentrations of nitrogen and (b) PXRD pattern of anatase 1 0 1 plane of undoped and doped samples.

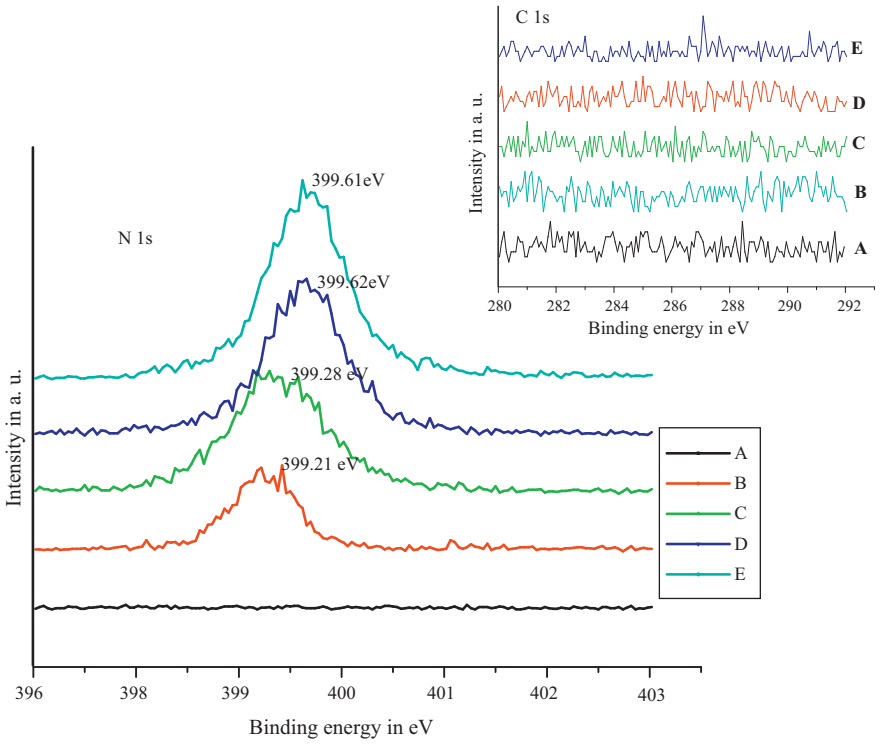

Fig. 2. XPS of N 1s and the inset figure shows the high-resolution C 1s XPS spectra for (A) TiO_2, (B) 0.05, (C) 0.1, (D) 0.15 and (E) 0.2 at.% nitrogen doped samples.

2.3. Characterization of the catalyst

The PXRD patterns of samples were studied using Philips PW/1050/70/76. X-ray diffractometer was operated at 30 kV and 20 mA. Cu Kα is used as a source with nickel filter at a scan rate of 2°/min. To get the X-ray diffraction line broadening, the reflection peaks were recorded with slow scanning speed (1/2°/min) with chart speed of 1 mm/min and low counts per second (CPS) were employed. X-ray photoelectron spectra of these materials were recorded with ESCA-3 Mark II spectrometer (VG Scientific Ltd., U.K.) using Al Kα radiation (1486.6 eV). FTIR spectra (NICOLLET IMPACT 400 D FTIR spectrometer) of the TiO_2 and $TiO_{2-x}N_x$ samples in the range 400–4500 cm^{-1} were measured using potassium bromide as the reference. The Diffuse Reflectance Spectra (DRS) of the photocatalyst samples were obtained using UV–visible spectrophotometer (Schimadzu-UV 3101 PC UV-VIS-NIR), with $BaSO_4$ as the reference. Surface morphology was analyzed by SEM analysis using JSM840 microscope operating at 25 kV on specimen upon which a thin layer of gold had been evaporated. An electron microprobe in the EDX mode was employed to obtain quantitative information on the amount of the non metal ion incorporated into the TiO_2 lattice. The specific surface area of the powders were measured by dynamic Brunner–Emmet–Teller (BET) method in which N_2 gas was adsorbed at 77 K using Digisorb 2006 surface area, pore volume analyzer Nova Quanta Chrome Corporation instrument multipoint BET adsorption system. Photoluminescence (PL) spectra of the generated 2-hydroxyterephthalic acid were measured on a Hitachi F-7000 fluorescence spectrophotometer. GC–MS analysis (using GC-MS-QP-5000 Shimadzu) and Thermo Electron Trace GC ultra coupled to a DSQ mass spectrometer equipped with an Alltech ECONO-CAP-EC-5 capillary column (30 m × 0.25 mm i.d. × 0.25 mm film thickness) was used. Pure helium was used as the carrier gas at a flow rate of 1.2 ml/min. The injector/transfer line/trap temperature was at 220/250/200 °C respectively. Electron impact ionization was carried out at 70 eV.

2.4. Experimental

Artificial light source of 125 W medium pressure mercury vapor lamp with the photon flux of 7.75 mW/cm^2 whose wavelength of emission is around ~370 nm is used as UV source. All the experiments were carried out in a circular borosilicate glass reactor with expose area of 176 cm^2. Photocatalysis under solar light was performed between 11 am and 2 pm during the summer season in the months of April–June at Bangalore, India. The latitude and longitude are 12.58N and 77.38E respectively. The average solar intensity was found to be 0.753 kW m^{-2} (using solar radiometer). The intensity of solar light was concentrated by convex lens and the reaction mixture was exposed to this concentrated solar light. The extent of generation of hydroxyl radicals (•OH) on the surface of

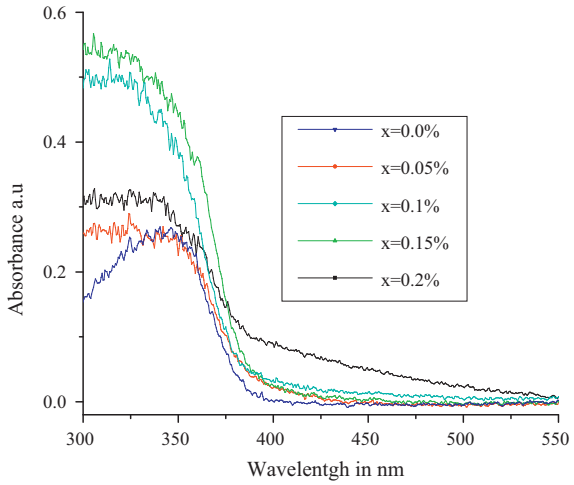

Fig. 3. UV–visible absorption spectra of TiO_2 and $TiO_{2-x}N_x$ samples.

$TiO_2/TiO_{2-x}N_x$ under UV/visible irradiation in the presence of electron acceptor is detected by a PL technique with terephthalic acid as a probe molecule as reported previously in the literature [27–30]. In a typical experiment 20 mg/L of Ph solution along with 400 mg/L of photocatalyst were used. The reaction mixture is stirred vigorously using magnetic stirrer for the entire time span of the experiment. The samples collected at different time intervals were centrifuged and filtered through 0.45 μm Millipore filter to remove the catalyst particles. The residual concentration of the Ph was determined by UV–vis spectroscopy in the range of 190–400 nm. The complete degradation was confirmed by UV–vis and GC–MS techniques.

3. Results and discussion

3.1. PXRD studies

The PXRD patterns of photocatalysts were indexed to anatase phase as shown in Fig. 1(a). However no N-derived peak was detected for NT photocatalyst. The average crystallite size (D) was calculated in accordance with Scherrer's formula using full width at half maximum (FWHM) data. $D = k\lambda/\beta\cos\theta$, where k is the constant (shape factor, ~0.9), λ is the X-ray wavelength (0.15418 nm), β is the full width at half maximum of the diffraction line and θ is the diffraction angle. The values of β and θ are taken for crystal plane 1 0 1. The peaks corresponding to 1 0 1 plane of the doped TiO_2 shifts slightly to higher values of 2θ on doping (Fig. 1(b)). The shift in the 2θ values of 1 0 1 plane in the doped samples with respect to SG was found to be 0.1204°, 0.1876°, 0.3557° and 0.3389° for NT1, NT2, NT3 and NT4 respectively. This shift is due to the replacement of high density oxygen atom (1.14 g/ml) by low density nitrogen atom (0.81 g/ml) in the TiO_2 lattice [31,32]. According to Ogale et al. [33] the marginal shift in the peak position to higher angle (lower d value) may have resulted due to the nitrogen incorporation into the TiO_2 matrix. Lower d value implies compressive strain, which may emanate from the differences in the bonding characteristics between nitrogen and oxygen. They suggested a significant modification in the electronic states, which takes place due to the replacement of oxygen by nitrogen on doping, leading to the substantial shift in the optical absorption towards the visible region. The results obtained show that the N^{3-} doping into the TiO_2 lattice effectively decrease the average crystal size as the concentration of nitrogen increases. The PXRD peaks corresponding to the crystal plane 1 0 1, 2 0 0 and 0 0 4 of anatase were selected to calculate the lattice parameters of TiO_2 and $TiO_{2-x}N_x$ by using the Bragg's equation $d_{(h\,k\,l)} = \lambda/2d\sin\theta$, where $d_{h\,k\,l}$ is the distance between the crystal planes of $h\,k\,l$, λ is the wavelength of the X-ray used, $h\,k\,l$ is the crystal plane index. Nitrogen doped TiO_2 samples shows slight change in '*a*' and '*c*'-axis. The shift in the peak position and the change in the lattice parameters indicate the nitrogen incorporation. These changes can be attributed to the internal strain developed due to the incorporation of nitrogen [31]. The calculated lattice parameters and the unit cell volume of all the samples are shown in Table 1.

3.2. XPS analysis

Fig. 2 shows the XPS spectra of N-doped TiO_2 and undoped TiO_2. A broad peak at 396–400 eV is observed for doped samples and no such signal was observed for undoped samples (Fig. 2). The peaks are excepted at 397–400 eV, which could be assigned to the typical N-doped TiO_2 as reported by several researchers [15,34]. This peak in the range of 396–397 eV can be attributed to nitrogen, replacing the oxygen in the crystal lattice of TiO_2 since the binding energy of Ti–N is 397 eV [17]. The observed peak at 399 eV in the present case for doped samples can be attributed to anionic N– in O–Ti–N linkages [17,34]. Nitrogen shows lower electronegativity value compared to oxygen. This leads to the reduction of electron density on the nitrogen. At the same time, there is an increase of the electron density on Ti due to the lower electronegativity of nitrogen compared with oxygen. This further testifies that nitrogen is incorporated into the lattice and substitutes for oxygen [17,35]. The inset in Fig. 2 shows the high resolution C 1s XPS spectra, indicating the absence of either elemental carbon (interstitial, C–O bond) or substituted carbon (substitutional, Ti–C bond) with binding energy around 285 and 281 eV for both doped and undoped samples. This confirms the absence of carbon in the doped samples. At higher calcination temperature carbon gets eliminated. The obtained results are also in accordance with the literature [36–38]. The composition in at.% for the various catalysts calculated from XPS analysis is summarized in Table 2.

3.3. UV–visible Diffused Reflectance Spectral (DRS) studies

DRS of SG and $TiO_{2-x}N_x$ samples are as shown in Fig. 3. The optical band edge of the $TiO_{2-x}N_x$ shows a remarkable red shift towards the visible region with respect to SG, due to the substitution of nitrogen at oxygen lattice site and mixing of 2p states of N and O resulting in the band gap narrowing [13,39]. The band gap energy (E_g) of these samples was estimated from the plot of square root of Kubelka–Munk function versus photon energy. SG shows optical absorption threshold at 380 nm corresponding to band gap of 3.26 eV. The absorption maximum and the corresponding band gap energies of all the samples are summarized in Table 1. The extent of red shift reaches a maximum at a dopant concentration of 0.2 at.% and the absorption peak is around 435 nm corresponding to the band gap of 2.86 eV. This narrowing in the band gap facilitate excitation of an electron from the valence band to the mid band gap state created by the dopant or from the dopant level to the conduction band in the doped metal oxide semiconductor, thereby increasing the photocatalytic activity of the material. It might be concluded that the observed new absorption edge can be related to the concentration of nitrogen in the doped samples. At the same time, the replacement of O^{2-} with N^{3-} would result in the formation of anion defects of the type oxygen vacancy (V_o) for the charge compensation. The anion defects may lead to visible light absorption ability of the sample. The optimum concentration of nitrogen in the TiO_2 lattice is found to be 0.15 at.% which shows higher rate of degradation. This is because the oxygen vacancies, which are created by the nitrogen incorporation facilitates the process of trapping the charge carriers. But these defects act adversely when they increase in the number by acting as recombination centers for the photogenerated charge carriers, with increase in the dopant concentration.

3.4. FTIR studies

FTIR spectra in the range of 400–4500 cm^{-1} of the SG and $TiO_{2-x}N_x$ were analyzed and are shown in Fig. 4(a). All the samples show relatively strong band at ~1630 cm^{-1} which can be attributed to the OH bending vibration [32] due to the surface hydroxyl groups. Peaks at 3400, 2930 and 2850 cm^{-1} were attributed to the Ti–OH bond [40]. The adsorbed water and hydroxyl ion content are crucial to the photocatalytic activity. The photogenerated holes on the catalyst surface reacts with hydroxyl ions producing hydroxyl radicals, which are powerful oxidants. The $TiO_{2-x}N_x$ samples show additional peaks at 1400, 1200, 1036 and 1160 cm^{-1} (as shown in Fig. 4(b)) which could be attributed to the bonds involving nitrogen atom embedded in to the TiO_2 matrix [41]. The peak observed at 600 cm^{-1} was ascribed to absorption bands of Ti–O and O–Ti–O. The peak at 1400–1450 cm^{-1} for nitrogen doped samples can be assigned to the bending vibration mode of the N–H band which might be formed by the dopant nitrogen reacting with the adsorbed

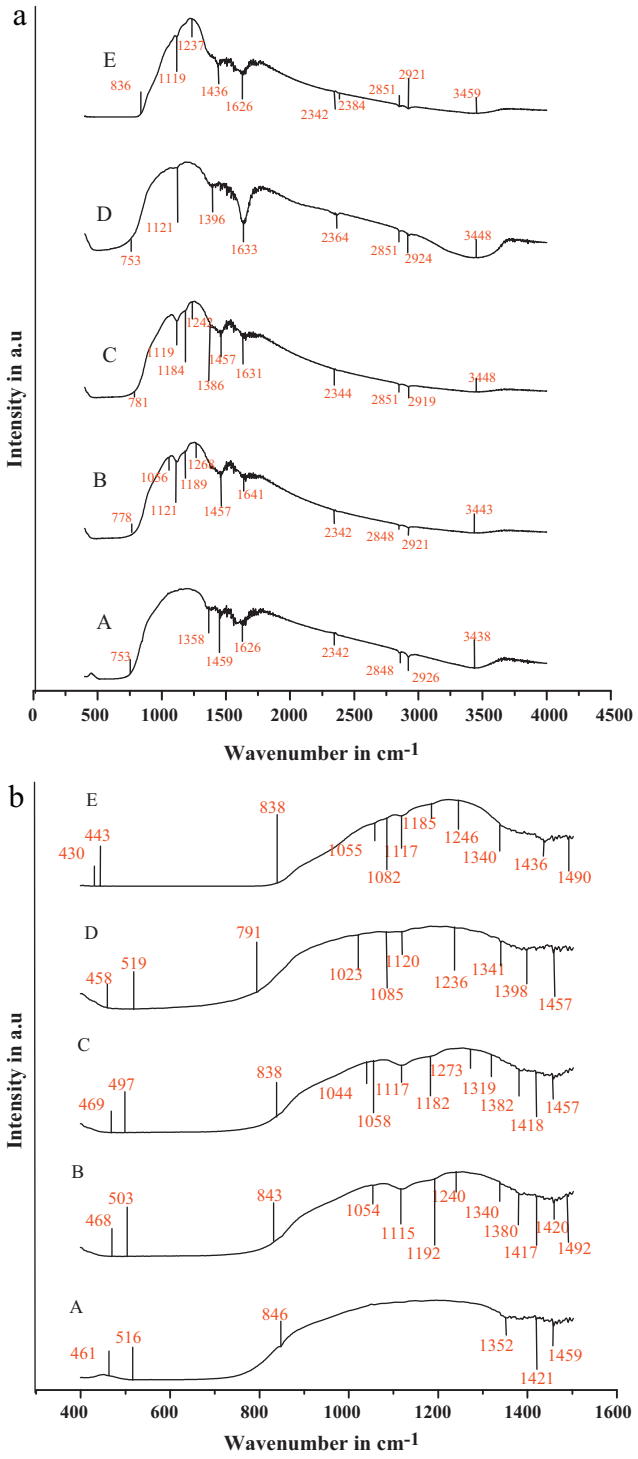

Fig. 4. (a) FTIR spectra of TiO_2 and $TiO_{2-x}N_x$ samples in the region 400–4500 cm^{-1} where (A) TiO_2, (B) NT1, (C) NT2, (D) NT3, and (E) NT4. (b) FTIR spectra of TiO_2 and $TiO_{2-x}N_x$ samples in the region 400–1500 cm^{-1} where (A) TiO_2, (B) NT1, (C) NT2, (D) NT3, and (E) NT4.

water [42]. The intensity of the N–H absorption peak increases with increasing the concentration of nitrogen. The peaks at 3696 and 1450 cm^{-1} may correspond to $-NH_2$ stretching and bending vibrations which was observed in all the doped photocatalysts. The typical characteristic band of urea is expected at 3210 cm^{-1} and this band is absent in all the samples [43], suggesting the absence of urea content which is efficiently removed in the calcinations process. The stretching vibration peaks at 3458 (Fig. 4(A)) and 516 cm^{-1}

Rate equations	Equation numbers
$r_{ap,\,Hp,\,solar,\,Ph} = 0.0039\,[SG]^{0.32}$	(14)
$r_{ap,\,HP,\,solar,\,Ph} = 0.0039\,[P25]^{0.36}$	(15)
$r_{ap,\,Hp,\,solar,\,Ph} = 0.0039\,[NT]^{0.42}$	(16)
$r_{ap,\,APS,\,UV,\,Ph} = 0.0039\,[SG]^{0.46}$	(17)
$r_{ap,\,APS,\,UV,\,Ph} = 0.0039\,[P25]^{0.51}$	(18)
$r_{ap,\,APS,\,UV,\,Ph} = 0.0039\,[NT]^{0.46}$	(19)
$r_{ap,\,HP,\,UV,\,Ph} = 0.0039\,[SG]^{0.45}$	(20)
$r_{ap,\,HP,\,UV,\,Ph} = 0.0039\,[P25]^{0.40}$	(21)
$r_{ap,\,HP,\,UV,\,Ph} = 0.0039\,[NT]^{0.40}$	(22)

Scheme 1. The rate expressions obtained for the effect of catalyst SG, P25 and NT3 photocatalysts loading along with HP as an electron acceptor under solar irradiation are Eqs. (14)–(16) and UV irradiation are Eqs. (20)–(22). Similarly the rate expressions obtained for the effect of catalyst SG, P25 and NT3 photocatalysts loading along with APS as an electron acceptor under solar irradiation are Eqs. (17)–(19) for the degradation of Ph.

(Fig. 4(B)) shift to lower wave numbers indicating the possible creation of oxygen vacancies due to the nitrogen doping at the grain boundaries [44]. The shifts observed in these two peaks could be attributed to the formation of N–Ti–O bond and as well as oxygen vacancies.

3.5. SEM and BET studies

SEM images in Fig. 5 show significant difference in surface morphology between the pure titania and doped titania samples. The obtained morphology demonstrates the multispheres structure. This morphology may also contribute to the high surface area in the doped samples. Surface area and porosity of the samples were determined from N_2 adsorption and desorption isotherm measured at liquid N_2 temperature are summarized in Table 1. The NT4 catalyst poses higher surface area (41 m^2/g) compared to other doped samples and undoped SG samples (18 m^2/g). The BET surface area of the doped samples increases with increase in dopant concentration. These results can be accounted in the following way: (i) higher surface area of doped samples compared to undoped TiO_2 is due to the controlled nucleation and controlled growth of crystallites, leading to the formation of well ordered structure. Nitrogen atom dopant prevents the aggregation of smaller crystallites, forming larger pores and increases the surface area [36,45]. (ii) The lattice strain because of the dopant incorporation in TiO_2 network decrease the grain growth rate. During nitrogen incorporation many particles get ruptured along the grain boundary. Parida and Naik [45] have also reported similar results for their nitrogen doped samples, they have reported decrease in the crystallite size with increase in the urea concentration. Similar results were also reported by Li et al.

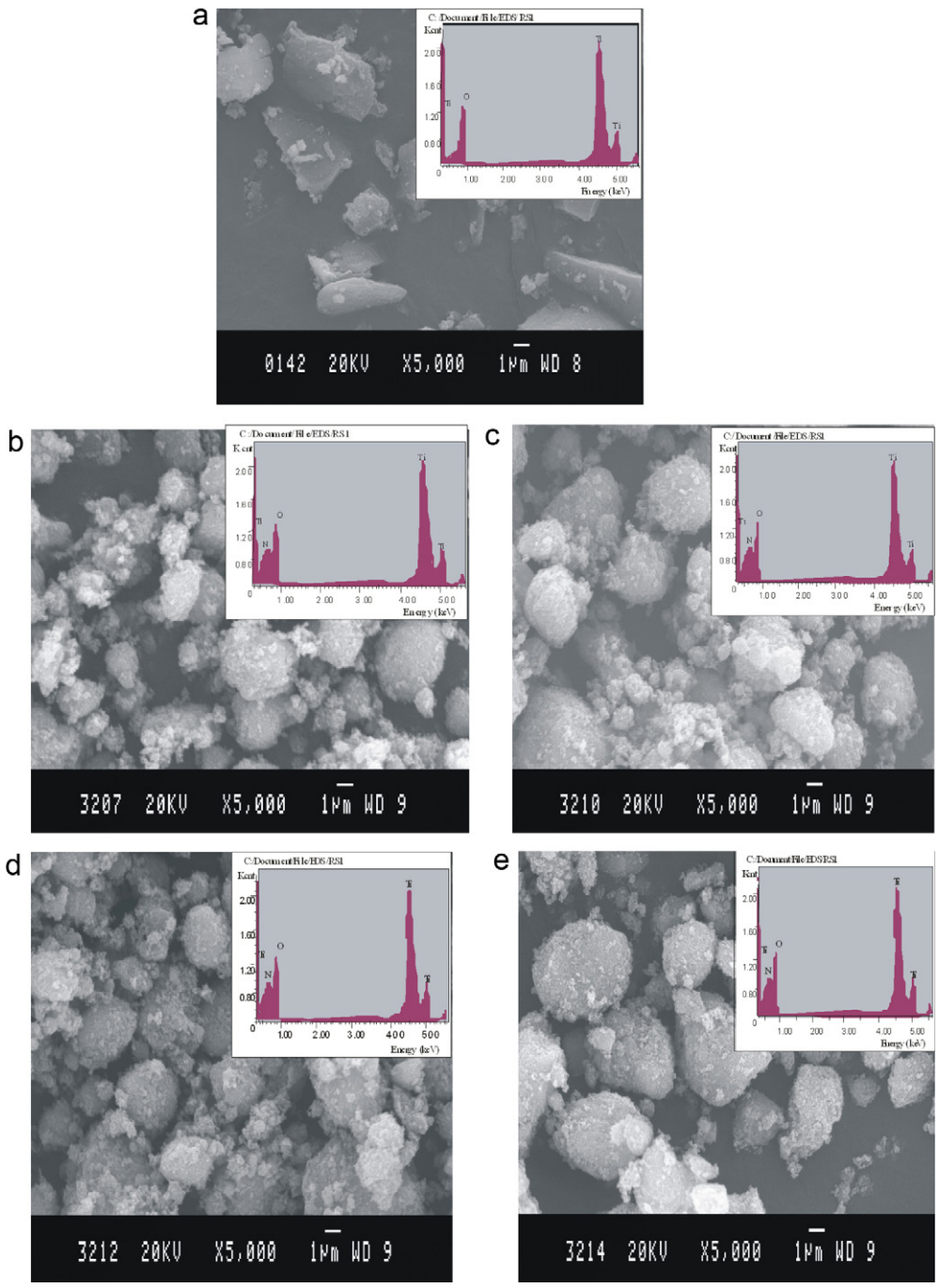

Fig. 5. SEM images of a reference undoped titania (a) and of the nitrogen doped titania samples NT1 (b), NT2 (c), NT3 (d) and NT4 (e) respectively, inset of the figure shows the corresponding EDX spectra.

[46] where nitrogen doped TiO_2 had smaller crystallite size and larger specific surface area with surface oxygen defects produced by nitrogen doping. EDX analysis confirmed the presence of dopant in the TiO_2 matrix and the spectra of all the samples are shown in the inset of Fig. 5.

3.6. Photocatalysis

It is generally accepted that, when semiconductor particles are irradiated by light with energy higher or equal to the band gap, an electron (e^-) in the valence band (VB) can be excited to the conduction band (CB) with the simultaneous generation of a hole (h^+) in the VB according to Eq. (2):

$$TiO_2/TiO_{2-x}N_x + h\nu \rightarrow TiO_2/TiO_{2-x}N_x(h^+ + e^-) \quad (2)$$

The photoinduced holes can be easily trapped by electronic donors, such as OH^- or organic radicals to further oxidize organic pollutants. Limitation in using $TiO_2/TiO_{2-x}N_x$ photocatalyst is the undesired electron/hole recombination process which, in the absence of proper electron acceptor or donor is extremely efficient and represents the major energy wasting step thus limiting the achievable degradation rate. One strategy to inhibit the electron–hole pair recombination is to add additional electron acceptors to the reaction. They could influence the reaction in the following ways: (1) they trap the photogenerated electrons

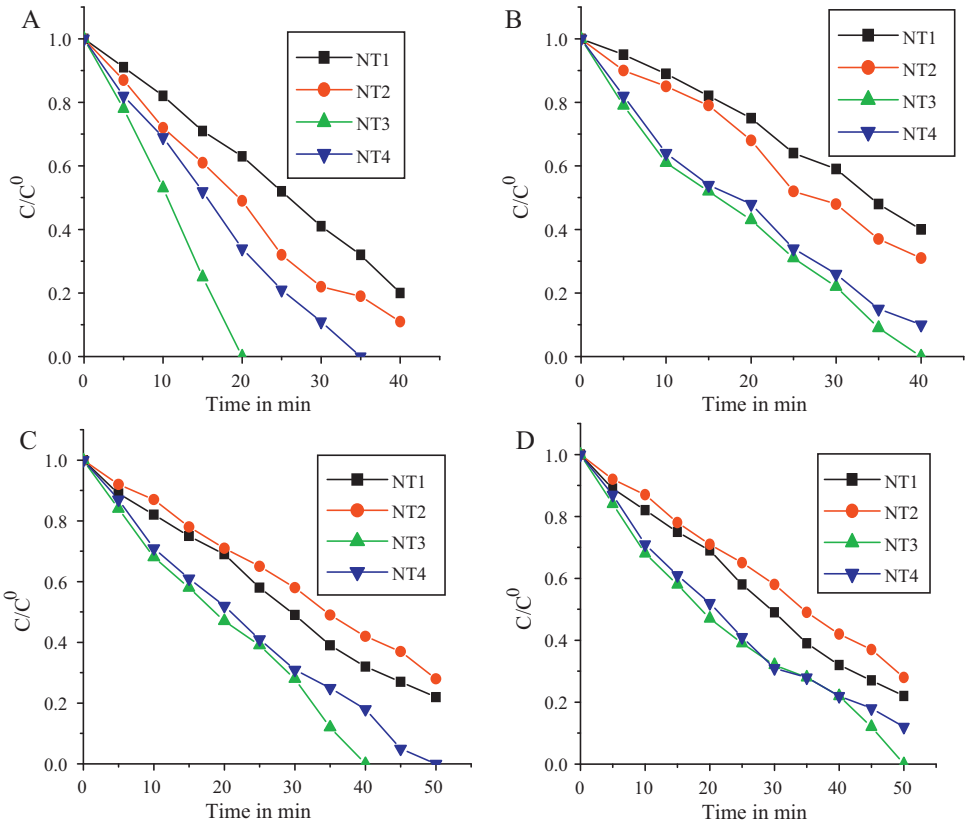

Fig. 6. Plots of C/C_0 versus time for the optimization NT3 photocatalyst at various processes. (a) NT/APS/Solar; (b) NT/HP/Solar; (c) NT/APS/UV; (d) NT/HP/UV ([NT] = 400 mg/L, [Ph] = 20 mg/L, [APS] = 100 mg/L and [HP] = 60 mg/L).

and consequently, avoid recombination. (2) They generate more hydroxyl radicals which posses high oxidizing capacity. (3) They increase the degradation rate of intermediate compounds. The use of HP as an electron acceptor in the photocatalytic process is quite well known. The effect of APS as an electron acceptor in presence of $TiO_2/TiO_{2-x}N_x$ on the photocatalytic process is attempted. This electron acceptor is known to generate hydroxyl radicals in addition to sulfate radicals which are crucial for the degradation of

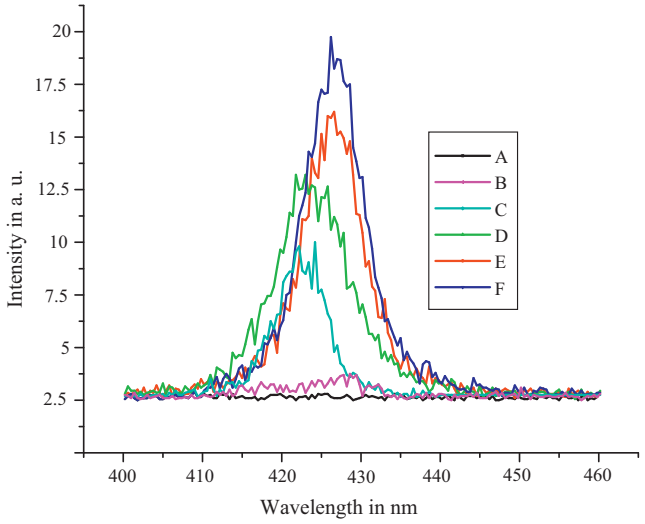

Fig. 7. PL spectral changes with visible-light irradiation on sample in a 1×10^{-4} M basic solution of terephthalic acid and PL spectra of samples for the system TiO_2 (A), $TiO_{2-x}N_x$ (B), TiO_2 + HP (C), TiO_2 + APS (D), $TiO_{2-x}N_x$ + HP (E) and $TiO_{2-x}N_x$ + APS (F) at a fixed time 15 min.

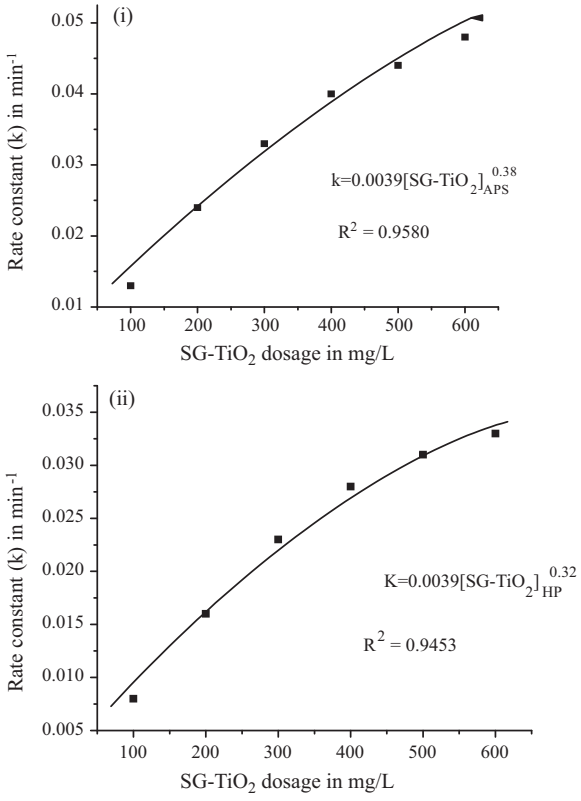

Fig. 8. (i) Plot of rate constant versus SG-TiO_2 dosage using APS as the oxidant. Under experimental conditions [Ph] = 20 mg/L and APS = 100 mg/L under. (ii) Plot of rate constant versus SG-TiO_2 dosage using HP as the oxidants under experimental conditions [Ph] = 20 mg/L and HP = 60 mg/L.

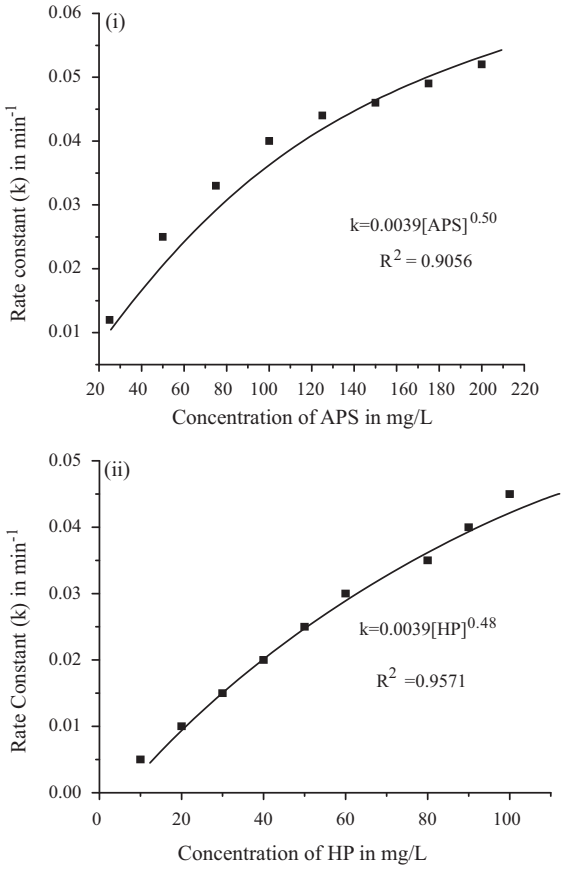

Fig. 9. (i) Plot of rate constant versus concentration of APS under the conditions [SG-TiO_2] = 400 mg/L and [Ph] = 20 mg/L. (ii) Plot of rate constant versus concentration of HP under the condition [SG-TiO_2] = 400 mg/L and [Ph] = 20 mg/L.

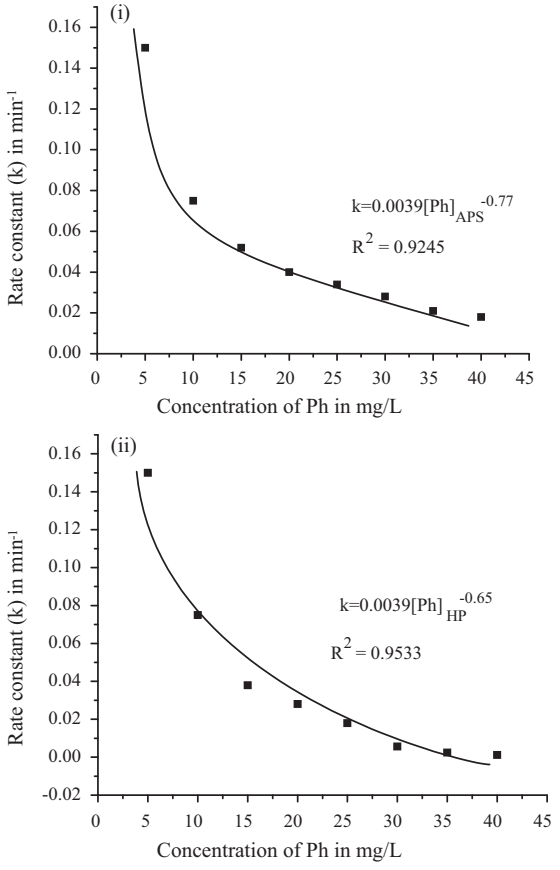

Fig. 10. (i) Plot of rate constant versus concentration of Ph using APS as the oxidant under experimental conditions [SG-TiO_2] = 400 mg/L and [APS] = 100 mg/L. (ii) Plot of rate constant versus concentration of Ph using HP as the oxidants ([SG-TiO_2] = 400 mg/L and [HP] = 60 mg/L).

pollutant (Eqs. (3)–(7)) [47]:

$$S_2O_8^{2-} + e^- \rightarrow SO_4^{2-} + SO_4^{\bullet -} \quad (3)$$

$$SO_4^{2-} + e^- \rightarrow SO_4^{2\bullet -} \quad (4)$$

$$SO_4^{\bullet -} + OH^- \rightarrow SO_4^{2-} + OH^{\bullet} \quad (5)$$

$$SO_4^{\bullet -} + H_2O \rightarrow SO_4^{2-} + OH^{\bullet} + H^+ \quad (6)$$

$$SO_4^{\bullet -} + RH \rightarrow \ldots \rightarrow SO_4^{2-} + CO_2 \quad (7)$$

APS is added to the reaction mixture in order to enhance the formation of hydroxyl radicals, which are thought to be the primary oxidizing species causing faster oxidation of organic molecules. The rates and the efficiency of photoassisted degradation of Ph are significantly improved by the addition of oxidizing agents [47–50]. Among the doped catalysts, NT3 shows better photocatalytic activity (Fig. 6(a)–(d)). The complete degradation of Ph takes place for the process NT3/APS/Solar in 20 min under the optimized conditions: [NT3] = 400 mg/L, [Ph] = 20 mg/L, [APS] = 100 mg/L and [HP] = 60 mg/L. This process is depicted in Fig. 6(a). The better photocatalytic performance of NT3 can be accounted in the following way: TiO_2 when doped with nitrogen, two N^{3-} ions can replace three O^{2-} ions to maintain the charge neutrality. This process can create an oxygen vacancy. When these oxygen vacancies are in appropriate number (at optimum dopant concentration), it facilitates the process of trapping the photogenerated charge carriers. But at higher dopant concentrations, these oxygen vacancies will probably act as recombination centers by capturing both the charge carriers. According to Irie et al. [13] these oxygen vacancies below the lower end of the conduction band acts as recombination centers thereby effectively decrease the degradation rate which is in agreement with the observed results.

3.7. Analysis of hydroxyl radicals (•OH) by photoluminescence (PL) technique

The generation of hydroxyl radicals is enhanced in the presence of oxidizing agents (APS/HP). This higher concentration of hydroxyl radical, enhances the degradation rate which could be observed in Fig. 6. Further the enhancement of hydroxyl radicals in the presence of oxidants is studied by the photoluminescence experiment [27–30]. The results have been incorporated in Fig. 7. It can be seen that a gradual increase in PL intensity at excitation wavelength at 425 nm shows the following order $TiO_2 < TiO_{2-x}N_x < TiO_2 + HP < TiO_2 + APS < TiO_{2-x}N_x + HP < TiO_{2-x}N_x + APS$.

3.8. Kinetic approach

3.8.1. Effect of catalyst loading

In order to the study the effect concentration of the catalyst on the photodegradation rate of the selected pollutant, experiments were conducted employing different concentrations of photocatalyst varying from 100 to 600 mg/L as shown in Fig. 8(i) and (ii) using APS and HP as the electron acceptor. Increase in the concentration of the catalyst causes increase in the initial reaction rate up to a value where it reaches a plateau. This concentration corresponds to the optimum amount of photocatalyst for better light absorption above which, light scattering may take place [51,52]. Further, high con-

Rate equations	Equation numbers
$r_{ap,\,SG,\,solar,\,Ph} = 0.0039\,[APS]^{0.50}$	(23)
$r_{ap,\,P25,\,solar,\,Ph} = 0.0039\,[APS]^{0.55}$	(24)
$r_{ap,\,NT,\,solar,\,Ph} = 0.0039[APS]^{0.71}$	(25)
$r_{ap,\,SG,\,UV,\,Ph} = 0.0039\,[APS]^{0.60}$	(26)
$r_{ap,\,P25,\,UV,\,Ph} = 0.0039\,[APS]^{0.66}$	(27)
$r_{ap,\,NT,\,UV,\,Ph} = 0.0039\,[APS]^{0.60}$	(28)
$r_{ap,\,SG,\,solar,\,Ph} = 0.0039\,[HP]^{0.48}$	(29)
$r_{ap,\,P25,\,solar,\,Ph} = 0.0039\,[HP]^{0.52}$	(30)
$r_{ap,\,NT,\,solar,\,Ph} = 0.0039\,[HP]^{0.61}$	(31)
$r_{ap,\,SG,\,UV,\,Ph} = 0.0039\,[HP]^{0.65}$	(32)
$r_{ap,\,P25,\,UV,\,Ph} = 0.0039\,[HP]^{0.59}$	(33)
$r_{ap,\,NT,\,UV,\,Ph} = 0.0039\,[HP]^{0.57}$	(34)

Scheme 2. The rate expressions obtained for the effect of concentration of APS as a electron acceptor along with photocatalyst SG, P25 and NT an under solar irradiation are Eqs. (23)–(25) and UV irradiation are Eqs. (26)–(28). The rate expressions obtained for the effect of concentration of HP as a electron acceptor along with photocatalyst SG, P25 and NT an under solar irradiation are Eqs. (29)–(31) and under UV irradiation Eqs. (32)–(34) for the degradation of Ph.

centration of the catalyst leads to agglomeration (particle–particle interactions) which can result in the loss of surface area available for light absorption. Fig. 8 shows the optimum concentration of titania to be 400 mg/L. The degradation rate shows exponential behavior with respect to catalyst dosage when all the other reaction parameters are maintained constant. The degradation rate follows a non-linear empirical power-law relationship with catalyst dosage. The apparent reaction rate constants for the photocatalytic degradation of Ph in the presence of different dosages (100–600 mg/L) at an optimum concentration of oxidant were evaluated from experimental data. In all the cases R^2 (correlation coefficient) values were higher than 0.9, which confirms the suitability of the proposed kinetic model for degradation of Ph:

$$r_{ap,APS,solar,Ph} \propto [SG]^{n} \quad (8)$$

where 'n' is an integer and '$r_{ap,\,APS,\,solar,\,Ph}$' represents the apparent rate constant where the subscript APS, solar, Ph implies the degradation of Ph using APS as an electron acceptor under solar light illumination. Fitting the experimental data we get the n value as 0.38:

$r_{ap,APS,solar,Ph} \propto [SG]^{0.38}$ or $r_{ap,APS,solar,Ph} = x[SG]^{0.38}$where x is a proportionality constant, which is arbitrarily chosen as 0.0039 to fit the experimental data.

$$r_{ap,APS,solar,Ph} = 0.0039[SG]^{0.38} \quad (9)$$

For the other P25 and NT photocatalysts the empirical rate equations obtained for the degradation of Ph using APS as an electron acceptor under solar light illumination are found to be:

$$r_{ap,APS,solar,Ph} = 0.0039[P25]^{0.38} \quad (10)$$

$$r_{ap,APS,solar,Ph} = 0.0039[NT]^{0.54} \quad (11)$$

The rate expressions for the process in which APS is used as an electron acceptor under UV light irradiation are summarized in Scheme 1. Similarly the rate expressions for the SG, P25 and NT3 photocatalysts along with HP as an electron acceptor under solar/UV light irradiation and the corresponding rate constant values for the process are depicted in Scheme 1 and Table 3.

3.8.2. Effect of initial concentration of electron acceptors

In this study the effect of initial concentration of electron acceptors such as APS and HP are investigated. These electron scavengers have been tested and shown to increase the reaction rate [53,54]. The ability of peroxydisulfate is attributed to the sulfate radicals which are very strong oxidizing agent (Eqs. (3)–(7)) [50,55]. Persulfate can generate free radicals like sulfate and hydroxyl radicals

Rate equations	Equation numbers
$r_{ap,\,SG,\,solar,\,APS} = 0.0039\,[Ph]^{-0.77}$	(35)
$r_{ap,\,P25,\,solar,\,APS} = 0.0039\,[Ph]^{-0.74}$	(36)
$r_{ap,\,NT,\,solar,\,APS} = 0.0039\,[Ph]^{-0.70}$	(37)
$r_{ap,\,SG,\,UV,\,APS} = 0.0039\,[Ph]^{-0.65}$	(38)
$r_{ap,\,P25,\,UV,\,APS} = 0.0039\,[Ph]^{-0.72}$	(39)
$r_{ap,\,NT,\,UV,\,APS} = 0.0039\,[Ph]^{-0.84}$	(40)
$r_{ap,\,SG,\,solar,\,HP} = 0.0039\,[Ph]^{-0.92}$	(41)
$r_{ap,\,P25,\,solar,\,HP} = 0.0039\,[Ph]^{-0.97}$	(42)
$r_{ap,\,NT,\,solar,\,HP} = 0.0039\,[Ph]^{-0.93}$	(43)
$r_{ap,\,SG,\,UV,\,HP} = 0.0039\,[Ph]^{-0.89}$	(44)
$r_{ap,\,P25,\,UV,\,HP} = 0.0039\,[Ph]^{-0.81}$	(45)
$r_{ap,\,NT,\,UV,\,HP} = 0.0039\,[Ph]^{-0.78}$	(46)

Scheme 3. The rate expressions obtained for the effect of initial concentration of substrate Ph for APS as electron acceptor along with photocatalyst SG, P25 and NT under solar irradiation are Eqs. (35)–(37) and UV irradiation are Eqs. (38)–(40) light irradiation. Similarly the rate expressions obtained for the effect of initial concentration of substrate Ph for HP as electron acceptor along with photocatalyst SG, P25 and NT under solar irradiation are Eqs. (41)–(43) and UV irradiation are Eqs. (44)–(46).

Table 3
Rate constant for the degradation of Ph under UV light and solar light for three different photocatalysts using two electron acceptor HP and APS, where '*k*' is the rate constant calculated from the plot of $-\log C/C_0$ versus time ([photocatalysts] = 400 mg/L and [Ph] = 20 mg/L, [HP]/APS = 60/100 mg/L).

Process	Under UV light, k (min^{-1})		Under solar light, k (min^{-1})	
	APS	HP	APS	HP
SG-TiO_2	0.0626	0.0576	0.0401	0.0281
Degauss P-25	0.0839	0.0454	0.0601	0.0339
NT1	0.0321	0.0282	0.0791	0.0325
NT2	0.0389	0.0294	0.0846	0.0412
NT3	0.0646	0.0404	0.1031	0.0490
NT4	0.0543	0.0371	0.0892	0.0379

which provide free radical mechanism similar to hydroxyl radicals in the case of HP. Sulfate radical is one of the strongest oxidizing species in aqueous media with a redox potential of 2.6 V which is next only to the hydroxyl free radical whose redox potential is 2.8 V. The sulfate radical anions produced in the case of APS shows various possible reaction mechanisms in the process of mineralization: (i) sulfate radical can abstract a hydrogen atom from the saturated carbon; (ii) it can possibly add to the unsaturated compounds; (iii) it can remove an electron from the anions and neutral molecules [41,56]. These attributes make persulfate an important viable option as an electron acceptor for a broad range of contaminants. The influence of electron acceptor on the degradation was investigated by maintaining the other reaction parameters constant (catalyst dosage = 400 mg/L, Ph concentration = 20 mg/L). The concentration of APS was varied from 20 to 200 mg/L. The degradation rate increases with increase in APS concentration from 20 to 100 mg/L. Further addition of APS does not show any noticeable change in the degradation rate as shown in Fig. 9(i) and it is optimized to 100 mg/L. Similarly the concentration of HP was varied from 10 to 100 mg/L. The degradation rate increases with increase in HP concentration from 10 to 60 mg/L. Further addition of HP does not show any noticeable change in the degradation rate as shown in Fig. 9(ii) and it is optimized to 60 mg/L. The non-linear relation between the rate of degradation of Ph with the change in the concentration of the electron acceptor APS/HP under solar/UV light irradiation using empirical power-law type relationship is given in Scheme 2. Beyond the optimum concentration of the electron acceptor, the rate of degradation decreases for both the oxidants. As the number of free radicals increases with increase in the concentration of oxidant, the close proximity and their frequent collision may lead to the recombination thereby decreasing the rate of degradation.

Rate equations	Equation numbers
$r_{ap,Solar} = 0.0041[SG]^{0.68}[APS]^{0.50}[Ph]^{-0.77}$	(47)
$r_{ap,solar} = 0.0039[P25]^{0.40}[APS]^{0.55}[Ph]^{-0.74}$	(48)
$r_{ap,solar} = 0.0041[NT]^{0.54}[APS]^{0.71}[Ph]^{-0.70}$	(49)
$r_{ap,solar} = 0.0040[SG]^{0.32}[HP]^{0.42}[Ph]^{-0.65}$	(50)
$r_{ap,solar} = 0.0040[P25]^{0.36}[HP]^{0.52}[Ph]^{-0.72}$	(51)
$r_{ap,solar} = 0.0041[NT]^{0.42}[HP]^{0.61}[Ph]^{-0.84}$	(52)
$r_{ap,UV} = 0.0039[SG]^{0.46}[APS]^{0.60}[Ph]^{-0.92}$	(53)
$r_{ap,UV} = 0.0034[P25]^{0.51}[APS]^{0.66}[Ph]^{-0.97}$	(54)
$r_{ap,UV} = 0.0039[NT]^{0.48}[APS]^{0.60}[Ph]^{-0.93}$	(55)
$r_{ap,UV} = 0.0039[SG]^{0.45}[HP]^{0.65}[Ph]^{-0.89}$	(56)
$r_{ap,UV} = 0.0045[P25]^{0.40}[HP]^{0.59}[Ph]^{-0.81}$	(57)
$r_{ap,UV} = 0.0045[P25]^{0.39}[HP]^{0.57}[Ph]^{-0.78}$	(58)

Scheme 4. The individual rate equations formulated for the photocatalysts along with APS as an electron acceptor under solar irradiation are Eqs. (47)–(49) and UV irradiation Eqs. (50)–(52). Similarly rate equations formulated for the photocatalysts along with APS as an electron acceptor under solar irradiation are Eqs. (53)–(55) and UV irradiation Eqs. (56)–(58) are formulated for the photocatalysts SG, P25 and NT.

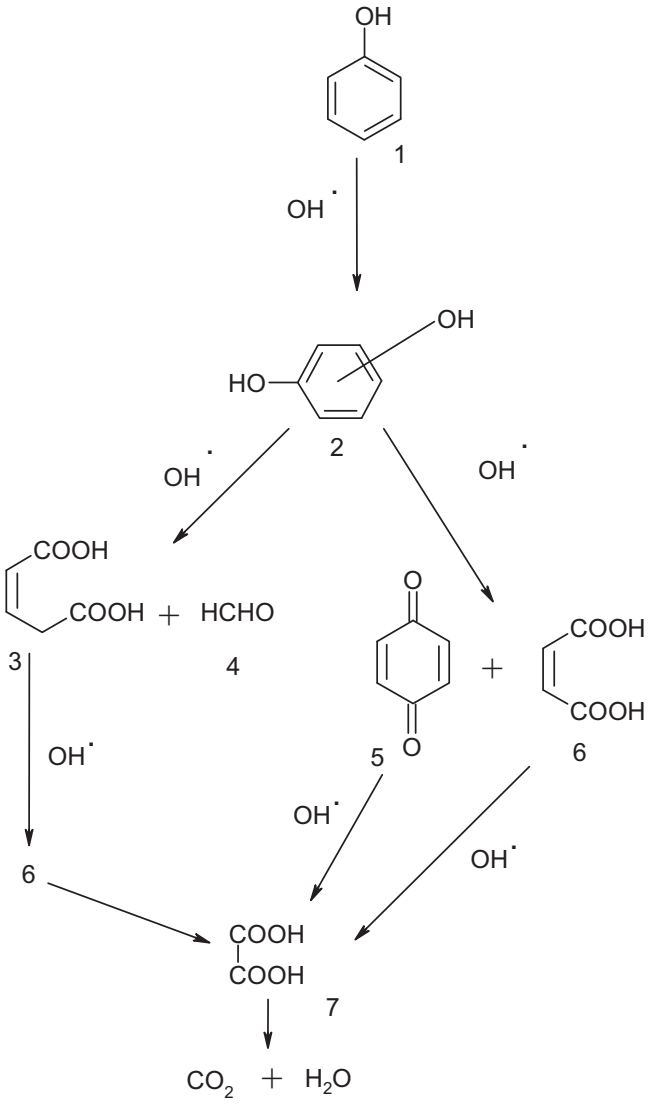

Scheme 5. Probable degradation mechanism for Ph under experimental condition for the best system ([NT3] = 400 mg/L, [APS] = 100 mg/L and [Ph] = 20 mg/L).

3.8.3. *Effect of initial concentration of substrate Ph*

It is important both from mechanistic and from application point of view to study the dependence of substrate concentration on

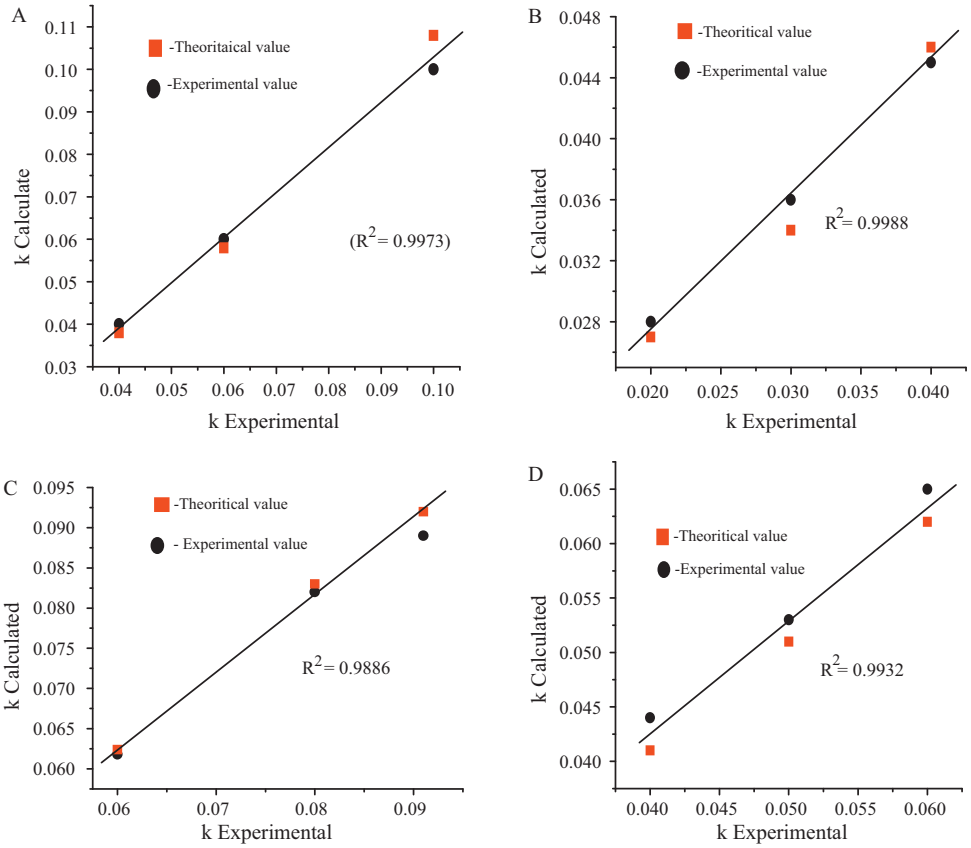

Fig. 11. Plots of calculated rate constant versus experimental rate constant. Where (a) using APS as the oxidant under UV light irradiation, (b) using HP as the oxidant under UV light irradiation, (c) using APS as the oxidant under solar light irradiation and (d) using HP as the oxidant under solar light irradiation.

the photocatalytic degradation rate. Change in the initial Ph concentration affects the degradation process significantly. Therefore experiments were performed at different initial Ph concentrations (10–200 mg/L) by maintaining the other reaction parameters constant in the presence of APS/HP as an electron acceptor are shown in Fig. 10(i) and (ii). Beyond this optimum concentration of Ph (20 mg/L) the degradation rate decreases. This may be due to the fact that, as the Ph concentration is increased, the concentration of the free radicals does not increase proportionally (since the concentration of electron acceptor and the amount of photocatalyst are held constant). High Ph concentration prevents the UV/solar light penetration into the depth by screening effect, thereby decreasing the rate of generation of hydroxyl radicals which are crucial for the degradation process. Additionally as the concentration of model pollutant increases, more and more molecules get adsorbed on the surface of the catalyst, preventing the process of photon absorption for the photogeneration of charge carriers. Further relative amounts of $OH^{\bullet}$ and $O_2^{\bullet -}$ on the surface of the catalyst do not increase as the intensity of the light and amount of catalyst are held constant, consequently the degradation efficiency of the model pollutant decreases. The non-linear relations involving the change in the concentration of the Ph, for the photocatalysts SG, P25 and NT3 along with APS/HP as an electron acceptor under solar/UV light irradiation are proposed in Scheme 3.

3.9. Development of overall rate equations

The photocatalytic degradation of Ph follows first order reaction with respect to Ph concentration which can be formulated as follows:

$$\frac{-d[\mathrm{Ph}]}{dt} = k\,[\mathrm{Ph}] \tag{12}$$

where k is rate constant for degradation of Ph.

But the rate critically depends on several factors like dosage of catalyst, type and concentration of electron acceptor and also on the initial concentration of the Ph which can be represented in the following way:

$$r = k[\mathrm{catalyst}]^a[\mathrm{oxidants}]^b[\mathrm{Ph}]^c \tag{13}$$

With non linear regression analysis the values of a, b and c are obtained as discussed in the previous sections. The individual rate equation is formulated for the photocatalyst SG, P25 and NT along with APS/HP as an electron acceptor under solar/UV light irradiation (Scheme 4). The plots of experimentally observed rate constant values versus theoretically calculated values are shown in Fig. 11. The results from the plot reveal that the proposed kinetic model is in good agreement with the observed experimental values which are summarized in Table 4. This model attempts to provide the information about the effect of exact operational parameters.

3.10. GC–MS analysis for the degradation of Ph

The generated hydroxyl radicals attack the Ph molecule leading to the formation of dihydroxy benzene (2) which is confirmed by the presence of m/z peaks at 110 (relative abundance [RA]: 42, retention time [Rt]: 10.4 min). Further degradation proceeds through the cleavage of dihydroxy benzene (2). After 15 min of UV irradiation m/z peaks at 130 (R_A: 54; Rt: 16.6 min) and 30 (R_A: 42; Rt: 28.6 min) corresponding to the formation of Pent 2-enedioic

Table 4
Comparison of theoretical and experimental rate constants for the degradation of Ph under UV/solar light for different processes under the condition ([photocatalysts] = 400 mg/L and [Ph] = 20 mg/L, [HP]/APS = 60/100 mg/L).

Process	Under UV light k (min^{-1})		Under solar light k (min^{-1})	
	Theoretical	Experimental	Theoretical	Experimental
Ph/SG/APS	0.0626	0.0618	0.0402	0.0397
Ph/P25/APS	0.0839	0.0824	0.0601	0.0592
Ph/NT3/APS	0.0635	0.0627	0.1031	0.1021
Ph/SG/HP	0.0576	0.0570	0.0281	0.0276
Ph/P25/HP	0.0454	0.0475	0.0339	0.0334
Ph/NT3/HP	0.0467	0.0458	0.0491	0.0487

acid (3) and formaldehyde (4) are observed. Few low intense peaks at 108 and 116 (R_A: 49; Rt: 6.8 min) were accounted as benzoquinone (5) and maleic acid (6). The decarboxylation of maleic acid (6) and ring opening of hydroquinone (5) results in the formation of oxalic acid (7) corresponding to the m/z peak at 90 (R_A: 64; Rt: 18.2 min). During photodegradation process formation of the two main intermediates of dihydroxy benzene (2), benzoquinone (5) is well agreement with the previously reported results [57]. Decarboxylation of oxalic acid further leads to the formation of carbon dioxide and water molecule. Based on the intermediates obtained, probable degradation mechanism has been proposed (Scheme 5).

4. Conclusion

The PXRD peaks corresponding to 1 0 1 plane of the doped TiO_2 shift slightly to higher values of 2θ on doping. The nitrogen doped TiO_2 samples shows red shift in the visible region. The surface area and morphology of the doped samples show prominent changes. Among doped catalysts, NT3 (with 0.15 at.% of nitrogen) shows better photocatalytic activity for the degradation of Ph under solar light. The activity of NT3 is compared with the SG and P25 in the presence of two symmetrical peroxides HP and APS as electron acceptors. A kinetic model was developed based on the non-linear regression analysis for the degradation of Ph. The influence of various reaction parameters like catalyst dosage, concentration of electron acceptor and initial concentration of Ph are investigated in detail. APS was proved to be a better electron acceptor compared to HP. Photoluminescence technique revealed the higher extent of hydroxyl radicals produced on TiO_2 and $TiO_{2-x}N_x$ (NT) surface in the presence of oxidants under UV/solar light irradiation. The theoretically calculated rate constant values were well in agreement with the experimentally obtained values justifying the significance of mathematical model. This model crucially provides the information about the exact operational parameters.

Acknowledgements

Authors greatly acknowledge the UGC Major Research Project (2007-2010) and Department of Science and Technology, Government of India for the financial assistance.

References

[1] L. Cermenati, P. Pichat, C. Guillard, A. Albini, J. Phys. Chem. B 101 (1997) 2650–2658.
[2] J. Yu, H. Yu, B. Cheng, C. Trapalis, J. Mol. Catal. A: Chem. 249 (2006) 135–142.
[3] J. Yu, L. Zhang, B. Cheng, Y. Su, J. Phys. Chem. C 111 (2007) 10582–10589.
[4] J. Yu, W. Liu, H. Yu, Cryst. Growth Des. 8 (2008) 930–934.
[5] J.G. Yu, Y.R. Su, B. Cheng, Adv. Funct. Mater. 17 (2007) 1984–1990.
[6] J. Yu, G. Wang, B. Cheng, M. Zhou, Appl. Catal. B: Environ. 69 (2007) 171–180.
[7] L. Palmisano, V. Augugliaro, A. Sclafani, M. Schiavello, J. Phys. Chem. 92 (1988) 6710–6713.
[8] C. Martin, I. Martin, V. Rives, L. Palmisano, M. Schiavello, J. Catal. 134 (1992) 434–444.
[9] L.G. Devi, S.G. Kumar, B.N. Murthy, N. Kottam, Catal. Commun. 10 (2008) 794–798.
[10] L.G. Devi, B.N. Murthy, Catal. Lett. 125 (2008) 320–330.
[11] M. Zhou, J. Yu, B. Cheng, J. Hazard. Mater. 137 (2006) 1838–1847.
[12] Slamet, H.W. Nasution, E. Purnama, S. Kosela, J. Gunlazuardi, Catal. Commun. 6 (2005) 313–319.
[13] H. Irie, Y. Watanable, K. Hashimoto, J. Phys. Chem. B 107 (2003) 5483–5486.
[14] J.C. Yu, J. Yu, W. Ho, Z. Jiang, L. Zhang, Chem. Mater. 14 (2002) 3808–3816.
[15] S. Sakthivel, M. Janczarek, H. Kisch, J. Phys. Chem. B 108 (2004) 19384–19387.
[16] S. Sato, Chem. Phys. Lett. 123 (1986) 126–128.
[17] R. Asahi, T. Morikawa, T. Ohwaki, K. Aoki, Y. Taga, Science 293 (2001) 269–271.
[18] T. Ohno, M. Akiyoshi, T. Umebayashi, K. Asai, T. Mitsui, M. Matsumura, Appl. Catal. A 265 (2004) 115–121.
[19] M.A. Behnajady, N. Modirshahla, Photochem. Photobiol. Sci. 5 (2006) 1078–1081.
[20] M.A. Behnajady, R. Modirshahla, Hamzavi, J. Hazard. Mater. 133 (2006) 226–232.
[21] Y. Zang, R. Farnood, Appl. Catal. B: Environ. 57 (2005) 275–282.
[22] C. Galindo, P. Jacques, A. Kalt, Chemosphere 45 (2001) 997–1005.
[23] T. Sauer, G.C. Neto, H.J. Jose, R.F.P.M. Moreira, J. Photochem. Photobiol. A: Chem. 249 (2002) 147–154.
[24] L.G. Devi, K.E. Rajashekhar, K.S. Anantharaju, S.G. Kumar, J. Mol. Catal. A: Chem. 314 (2009) 88–94.
[25] L.G. Devi, G.M. Krishnaiah, J. Photochem. Photobiol. A: Chem. 121 (1999) 141–145.
[26] S. Chen, L. Chen, S. Gao, G. Cao, Chem. Phys. Lett. 413 (2005) 404–409.
[27] K. Ishibashi, A. Fujishima, T. Watanabe, K. Hashimoto, Electrochem. Commun. 2 (2000) 207–210.
[28] J. Yu, W. Wang, B. Cheng, B.-L. Su, J. Phys. Chem. C 113 (2009) 6743–6750.
[29] Q. Xiang, J. Yu, B. Cheng, H.C. Ong, Chem. Asian J. 5 (2010) 1466–1474.
[30] J. Yu, G. Dai, B. Huang, J. Phys. Chem. C 113 (2009) 16394–16401.
[31] Y. Wanga, Y. Huanga, W. Hob, L. Zhanga, Z. Zouc, S. Leeb, J. Hazard. Mater. 169 (2009) 77–87.
[32] L. Lin, R.Y. Zheng, J.L. Xie, Y.X. Zhu, Y.C. Xie, Appl. Catal. B: Environ. 76 (2007) 196–202.
[33] T.C. Jagadale, S.P. Takale, R.S. Sonawane, H.M. Joshi, S.I. Patil, B.B. Kale, S.B. Ogale, J. Phys. Chem. C 112 (2008) 14595–14602.
[34] C. Burda, Y. Lou, X. Chen, A.C.S. Samia, J. Stout, J.L. Gole, Nano Lett. 3 (2003) 1049–1051.
[35] H. Li, J. Li, Y. Huo, J. Phys. Chem. B 110 (2006) 1559–1565.
[36] X. Yang, C. Cao, L. Erickson, K. Hohn, R. Maghirang, K. Klabunde, Appl. Catal. B: Environ. 91 (2009) 657–662.
[37] X. Wang, S. Meng, X. Zhang, H. Wang, W. Zhang, Q. Du, Chem. Phys. Lett. 444 (2007) 292–296.
[38] Z. Shi, X. Ye, K. Liang, S. Gu, F. Pan, J. Mater. Sci. 22 (2003) 1255–1259.
[39] I. Justicia, P. Ordejon, G. Canto, J.L. Mozos, J. Fraxedas, G.A. Battiston, R. Gerbasi, A. Figureas, Adv. Mater. 14 (2002) 1399–1402.
[40] M.S.K. Kamal, I.Z. Mohamed, Powder Technol. 92 (1997) 233–239.
[41] E. Evgenidou, I. Konstantinou, K. Fytianos, I. Poulios, Water Res. 41 (2007) 2015–2027.
[42] J.W. Wang, W. Zhu, Y.Q. Zhang, S.X. Liu, J. Phys. Chem. C 111 (2007) 1010–1014.
[43] Q. Li, N. Zhao, W. Wei, Y. Sun, J. Mol. Catal. A: Chem. 270 (2007) 44–49.
[44] T. Ihara, M. Miyoshi, Y. Iriyama, O. Matsumoto, S. Sugihara, Appl. Catal. B: Environ. 42 (2003) 403–409.
[45] K.M. Parida, B. Naik, J. Colloid Interface Sci. 333 (2009) 269–276.
[46] Y. Li, C. Xie, S. Peng, G. Lu, S. Li, J. Mol. Catal. A: Chem. 282 (2008) 117–123.
[47] C. Kosmann, P.W. Bahnemann, M.R. Hoffmann, J. Photochem. Photobiol. A: Chem. 48 (1989) 161–169.
[48] E. Pelizzeti, C. Minero, Electrochim. Acta 38 (1993) 47–55.
[49] W. Bahnamann, M. Muneer, M.M. Haque, Catal. Today 124 (2007) 133–148.
[50] J. Fernandez, P. Maruthamuthu, J. Kiwi, J. Photochem. Photobiol. A: Chem. 161 (2004) 185–192.
[51] A.B. Prevot, M. Vincenti, A. Bianciotto, E. Pramauro, Appl. Catal. B: Environ. 22 (1999) 149–158.
[52] N. Daneshvar, D. Salari, A.R. Khataee, J. Photochem. Photobiol. A: Chem. 6239 (2003) 1–6.
[53] E. Evegenidou, K. Fytianos, I. Poulios, J. Photochem. Photobiol. A: Chem. 175 (2005) 29–38.
[54] E. Evegenidou, K. Fytianos, I. Poulios, Appl. Catal. B: Environ. 59 (2005) 81–89.
[55] S. Malato, J. Blanco, C. Richter, B. Braun, M.I. Maldonado, Appl. Catal. B: Environ. 17 (1998) 347–356.
[56] P. Neta, V. Madhavan, H. Zemel, R.W. Fessenden, J. Am. Chem. Soc. 99 (1977) 163–164.
[57] H. Wang, J. Li, X. Quan, Y. Wu, G. Li, F. Wang, J. Hazard. Mater. 411 (2007) 336–343.